Dual-field imaging polarimeter using liquid crystal variable retarders

Nathan J. Pust and Joseph A. Shaw

An imaging Stokes-vector polarimeter using liquid crystal variable retarders (LCVRs) has been built and calibrated. Operating in five bands from 450 to 700 nm, the polarimeter can be changed quickly between narrow (12°) and wide (~160°) fields of view. The instrument is designed for studying the effects of differing sky polarization upon the measured polarization of ground-based objects. LCVRs exhibit variations in retardance with ray incidence angle and ray position in the aperture. Therefore LCVR-based Stokes polarimeters exhibit unique calibration challenges not found in other systems. Careful design and calibration of the instrument has achieved errors within ±1.5%. Clear-sky measurements agree well with previously published data and cloudy data provide opportunities to explore spatial and spectral variations in sky polarization.

OCIS codes: 120.5410, 260.5430, 290.1310, 280.0280.

1. Introduction

The observed polarization signature of a ground-based object changes with variations of the polarization of the illuminating light. For polarization measurements to be useful in military and civilian applications, the degree to which this change occurs needs to be quantified (and polarized radiative transfer simulations need to be validated). Although ideal clear skies can be modeled using Rayleigh scattering theory, aerosol-laden and cloudy skies pose more difficulty.[1] In an effort to better quantify both the polarization changes in clear and cloudy skies and the corresponding target signature changes, we have developed a dual-field Stokes-vector imaging polarimeter. This imaging polarimeter operates in five 10 nm bands centered at 450, 490, 530, 630, and 700 nm. The instrument uses two different front lenses: a 300 mm telephoto and a 16 mm fisheye. The telephoto lens is used for measuring ground-based objects, while the fisheye lens is used to measure the polarization of the whole sky.

Previous Full Sky Polarimetric Imagers. A few full-sky polarimeters have been built previously, based on both single- and multiple-detector designs. The advantage of a multiple-detector design is its ability to take multiple images concurrently, thereby eliminating errors from changing scenes if the detectors are aligned perfectly. Changes in the input Stokes vector over the total exposure period cause errors in the reconstructed measurement. Consequently, to minimize errors induced by a changing scene, the successive measurements need to be taken quickly. A well-conditioned system matrix describing the polarization state of the instrument for each image is inverted and multiplied to the images to reconstruct the Stokes vector images. For reconstruction of the entire Stokes vector, the minimum number of images is four.

Horvath *et al.*[2] describe a system based on single-lens reflex (SLR) film cameras. A train of three cameras mounted next to each other is pointed toward the zenith. Each camera has its own fisheye lens and individually oriented polarizer (0°, 60°, and 120°). The developed film is scanned and polarimetric images computed. These color-film images are used to produce polarimetric data in three broad spectral bands concurrently. The disadvantages of this approach include inconvenience and uncertainties related to developing and scanning film exposed in different cameras. North and Duggin[3] developed a four-lens stereoscopic camera that was directed downward to view the full sky reflected in a dome mirror on the ground. This system also provided simultaneous images on film, and the stereoscopic camera assisted pixel alignment by use of lenses that were machined to point in the same direction. How-

The authors are with the Department of Electrical and Computer Engineering, 610 Cobleigh Hall, Montana State University, Bozeman, Montana 59717. J. A. Shaw's e-mail address is jshaw@montana.edu.

Received 14 November 2005; accepted 9 January 2006; posted 28 March 2006 (Doc. ID 65977).

0003-6935/06/225470-09$15.00/0

ever, the camera blocked a portion of the zenith sky and also relied on film processing and scanning to produce polarization images.

A more automated, real-time approach was taken by Voss and Liu,[4] who used a fisheye lens mounted on a CCD imager. Reimaging optics were used to reduce the image to the size of the CCD chip, which was smaller than the film for which the lenses were designed. Polarimetric data were obtained by exposing three images sequentially through three different polarizers mounted in a rotating filter wheel. In addition to the three polarizers, the filter wheel also included an open aperture for recording polarization-insensitive images. By alternately rotating the polarizer wheel and a spectral filter wheel, three Stokes parameters could be measured at four different wavelengths. The advantages of this system over film-based systems included capabilities of analyzing data quickly and recording coaligned images with a common optical system. Additionally, 10 nm spectral bands gave the polarimeter the ability to better recognize narrower, band-dependent polarimetric signatures across the visible spectrum. However, time taken to expose and download each frame, coupled with the time to rotate the polarizers, resulted in a 2 min measurement time per wavelength.[5] This delay would create large errors in images taken with moving clouds, thereby limiting measurements to slowly changing or clear skies.

The system we describe here attempts to build on the strengths of the Voss–Liu system while minimizing the total measurement time to allow for the study of more highly variable sky conditions. This system also has a front end that can be quickly changed from a fisheye to a telephoto format to observe narrow fields of view. Rather than using rotating polarization elements to generate Stokes images at each spectral band, this instrument relies on liquid crystal variable retarders (LCVRs) to electronically vary the polarization state of the light incident on a single CCD camera. This typically allows full Stokes images to be obtained in down to 0.4 s in each spectral channel (we still use a rotating filter wheel to change the spectral band).

2. System Design

The design of the instrument focused on four goals: (i) provide easily changeable optics to allow alternate views of narrow and full-sky fields of view; (ii) keep incidence angles on the polarization optics small to minimize problems caused by the incidence-angle-dependent LCVR variable retardance; (iii) optimize aberrations to provide image spot sizes smaller than or comparable to the pixel size; (iv) minimize acquisition time over each measurement.

A. Optical Design

In the system design, a polarimetric accuracy of 1% was desired. Eight-bit data have a quantization error of at least 0.39% (0.39% being when the data span the full dynamic range). This error could potentially cause polarization errors of ~1% with system matrix condition numbers of ~2; to eliminate this error, only cameras incorporating better than 8-bit data were considered. To meet the requirements of fast image acquisition, a DALSA 1M30 camera was chosen. This 1 Mpixel camera exhibits 12-bit data, frame speeds up to 30 frames per second, and download times that are much shorter than the exposure time. The aberration optimization was simplified by the use of 13 μm pixels, which are larger than the pixels in many other cameras.

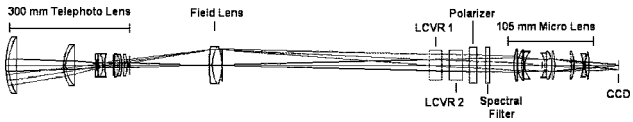

Fig. 1. Imaging polarimeter system layout, shown with a telephoto front lens.

Two lenses were selected for the front end, a Nikon 300 mm telephoto lens and a Nikon 16 mm fisheye lens. Since these lenses are designed to form a 35 mm film image (24 × 36 mm), the image needed reduction to fill the 13 mm CCD chip with the full fisheye field of view. Each front lens—telephoto and fisheye—was focused onto a field lens. This image was reimaged by a Micro-Nikkor 105 mm lens to the size of the 13 mm CCD chip. The selection of the 105 mm microlens also reduced the maximum ray incidence angle to 5°. In the telephoto system, the field lens [doublet, 120 mm effective focal length (EFL), 50 mm diameter] was chosen to eliminate vignetting on the 105 mm microlens. For the fisheye system, two of these same field lenses were necessary. Spectral filters of 10 nm wavelength centered at 450, 490, 530, 630, and 700 nm are used in the system. Figure 1 shows the layout with the telephoto front-end lens (lens prescriptions were obtained from Nikon patents[6–8]). The system with the fisheye lens looks similar.

Two Meadowlark LRC-300 temperature-controlled LCVRs, along with a fixed linear polarizer, were used to change the instrument polarization state. Effects of any polarization-dependent response of the detector and optics behind the polarizer are removed since only one polarization is seen beyond the polarizer. The retarders have been measured to completely change retardance in 55 ms. The time of measurement over the four images varies between 0.3 and 1.2 s (dependent on exposure time). Errors resulting from changing skies usually are negligible at this acquisition speed. When the LCVRs are in a stable state, the polarimeter accuracy is easily ±1.5%; however, the LCVRs tend to sometimes jump between states when the system is powered on and off, leading to errors of approximately 4% if the system is not recalibrated. Work is in progress to understand and remove these state changes.

B. Selection of Liquid Crystal Variable Retarder Retardances to Optimize Condition Number

A Mueller matrix is a 4 × 4 real matrix that describes the effect of an optical system on the Stokes vector S (i.e., the polarization state) of a light ray that passes through the system [Eq. (1)]:

$$\begin{bmatrix} S_0 \\ S_1 \\ S_2 \\ S_3 \end{bmatrix}_{\text{output}} = \begin{bmatrix} m_{00} & m_{01} & m_{02} & m_{03} \\ m_{10} & m_{11} & m_{12} & m_{13} \\ m_{20} & m_{21} & m_{22} & m_{23} \\ m_{30} & m_{31} & m_{32} & m_{33} \end{bmatrix} \begin{bmatrix} S_0 \\ S_1 \\ S_2 \\ S_3 \end{bmatrix}_{\text{input}}. \quad (1)$$

The Mueller matrix can represent one element of the system, or Mueller matrices can be multiplied to form one Mueller matrix for the whole system. For the purpose of this paper, all Mueller matrices will represent the entire system for one ray path. The overall objective of a Stokes polarimeter is to determine S, the Stokes vector of input light, from successive power measurements made with different instrument polarization states. As described in this section, we followed a procedure of selecting LCVR fast-axis angles and retardances to achieve an optimal system matrix. These fast-axis angles and retardances were used as first-order settings for the instrument. Calibration of the instrument then determined the actual values of the system matrix elements corresponding to these settings. Measurements from the resulting instrument are multiplied by the system matrix inverse to recover the input Stokes vector.

The system matrix, A, is the matrix that must be inverted to recover the input Stokes vector. Each of its four rows can be considered to be the first row of the instrument's Mueller matrix at a fixed polarimeter state. When four different images are taken with different instrument polarization states, the Mueller matrix changes for each measurement. The four rows of the system matrix A are the first rows from the four Mueller matrices corresponding to the four polarimeter states, as indicated in Eq. (2).

$$\begin{bmatrix} S_{01} \\ S_{02} \\ S_{03} \\ S_{04} \end{bmatrix} = \begin{bmatrix} a_{00} & a_{01} & a_{02} & a_{03} \\ a_{10} & a_{11} & a_{12} & a_{13} \\ a_{20} & a_{21} & a_{22} & a_{23} \\ a_{30} & a_{31} & a_{32} & a_{33} \end{bmatrix} \begin{bmatrix} S_0 \\ S_1 \\ S_2 \\ S_3 \end{bmatrix} = AS. \quad (2)$$

The retardances of the two LCVRs change the polarization state of the instrument. To reduce the amplification of image-exposure errors to Stokes-vector errors during Stokes-vector retrieval, the retardances of the LCVRs for each image should be chosen to minimize the condition number of the system matrix.[9–11] The condition number relates how the error is propagated; for example, if the condition number of A is 2, and the error in the exposure is 1%, the error in the Stokes parameter is expected to be 2%. Optimization for this instrument followed the work of Tyo.[10] The MATLAB (version 7.0.4) Optimization Toolbox (3.0.2) was used to optimize the fixed fast-axis orientation angle (with respect to the fixed linear polarizer axis) and the set of four retardances for each LCVR, with the LCVRs modeled as perfect retarders. This generates ten variables that are optimized to yield a minimum value of the system matrix condition number. Retardance values were constrained from 0° to 180° (half-wave retardance), although this is not strictly necessary. Many different sets of rotation angles and retardance angles with equivalent condition numbers could be found by varying initial conditions of the optimization. The set we chose to implement is shown in Table 1.

Table 1. Retarder Settings for Two-LCVR Polarimeter

	Retarder1	Retarder2
Fast axis fixed rotation angle	115.0°	45.0°
retardance angles		
Image 1 (Polarimeter state 1)	150.5°	105.2°
Image 2 (Polarimeter state 2)	27.7°	180.0°
Image 3 (Polarimeter state 3)	180.0°	15.4°
Image 4 (Polarimeter state 4)	18.17°	64.77°
Condition number (2 norm)	1.82	

The next step in the procedure is to calibrate the instrument to determine the actual values for the 16 system-matrix elements. However, before we proceed with the calibration discussion, we will first discuss the applicability of the Mueller matrix technique for our optical system whose response varies with incidence angle. The retardance and equivalent rotation angles for LCVRs have been shown to change according to incidence angle.[12] In an imaging system using LCVRs, each ray that forms the image will have a different retardance and rotation angle, causing apparent depolarization in the system. Therefore optimization using a perfect retarder model for the LCVRs only obtains a first-order approximate system matrix. Depolarization in the imaging system will change the system matrix from the ideal and increase the condition number of the system. In fact, only under certain constraints is a Mueller matrix—and therefore the system matrix—representation even valid for an imaging system.

C. Use of Mueller Matrices to Describe Imaging Systems

For most Stokes imaging systems using rotating polarizers and wave plates, the Mueller matrix of the system does not change significantly across the optical aperture. All ray paths to the image plane can be therefore summarized by one Mueller matrix. In LCVRs, the retardance and rotation angle of the birefringence can vary significantly according to the incidence angle of the ray, so different ray paths must be described by different Mueller matrices. In an imaging system using LCVRs, each ray converging on an image point will necessarily exhibit a slightly different Stokes vector, and the superposition of these rays causes apparent depolarization. (This effect is sometimes called polarimetric aberration, but it appears as depolarization. For simplicity, it is called depolarization in the remainder of this paper.) Therefore a LCVR used in an imaging system cannot be modeled as a perfect retarder. For proper calibration, it is desired to use the Mueller calculus to describe the system with LCVRs. Can an equivalent Mueller matrix for an imaging system with depolarization—in this case a LCVR system—be found? If so, will the condition number be significantly reduced by the depolarization?

Equation (3) shows the Mueller matrix for one ray (numbered 1) through the system.

$$\begin{bmatrix} S_0 \\ S_1 \\ S_2 \\ S_3 \end{bmatrix} = \begin{bmatrix} m_{00} & m_{01} & m_{02} & m_{03} \\ m_{10} & m_{11} & m_{12} & m_{13} \\ m_{20} & m_{21} & m_{22} & m_{23} \\ m_{30} & m_{31} & m_{32} & m_{33} \end{bmatrix} \begin{bmatrix} S_{0\text{ray}} \\ S_{1\text{ray}} \\ S_{2\text{ray}} \\ S_{3\text{ray}} \end{bmatrix} = M_1 S_1. \quad (3)$$

Assuming geometrical optics is a good approximation, the Stokes vector at the image point can be represented by a sum of the Stokes vectors for each ray, as illustrated in Eq. (4),

$$\begin{bmatrix} S_{0\text{total}} \\ S_{1\text{total}} \\ S_{2\text{total}} \\ S_{3\text{total}} \end{bmatrix} = M_1 S_1 + M_2 S_2 + M_3 S_3 + \cdots + M_N S_N, \quad (4)$$

where each number, 1, 2, . . . , N, represents a ray path through the system, and each S represents the Stokes vector for each ray (normalization is achieved by considering each S to carry the fraction of total power appropriate for each ray). For our instrument, every object is effectively located at infinity. The ray cone for any object will be the same in the instrument—the rays will always follow the same path. Also, since we are a long distance from the object, the wavefront across the aperture can be assumed to be uniform. Therefore the number of rays and the position of those rays in the imager will be constant, and the Stokes vector for all the rays will be the same. Under these conditions, Eq. (5) shows that an equivalent Mueller matrix can be found for each image point:

$$\begin{bmatrix} S_{0\text{total}} \\ S_{1\text{total}} \\ S_{2\text{total}} \\ S_{3\text{total}} \end{bmatrix} = (M_1 + M_2 + M_3 + \cdots + M_N) S^{(1)} = M\, S_{\text{input}}, \quad (5)$$

where $S^{(1)} = S^{(2)}, \ldots, = S^{(N)} =$ Stokes vector for each ray path $= S_{\text{input}}$, and M is the equivalent Mueller matrix for the image point for any N rays.

This treatment shows that under these assumptions the depolarization is systematic. Therefore the depolarization can be compensated for in the system calibration. It is just a matter of how much noise is amplified (shown by an increased system condition number). Notice that these assumptions necessarily have three consequences. First, each image point can have a different equivalent Mueller matrix associated with it. Therefore every pixel in the system must be calibrated separately. Second, the system must be calibrated separately for each $f/\#$ since changes in the ray cone will change the calibration. Third, the focus of the instrument cannot be changed without changing the calibration.

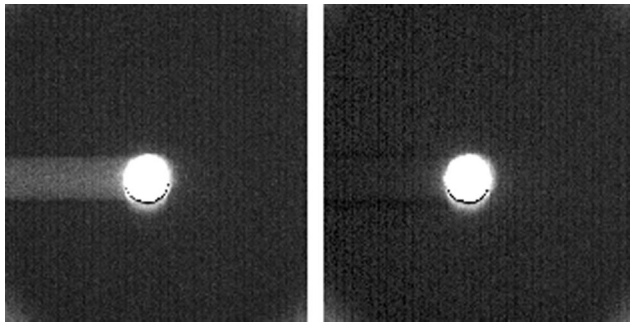

Fig. 2. Example of (left) row–column cross talk in an image with extreme contrast and (right) corrected image.

3. System Calibration

For each image, dark current is removed by subtracting a stored dark image at an exposure of 50 ms. Because longer exposures slightly increase the dark current, an exposure-dependent uniform correction is also subtracted from the image (experiments repeated weeks apart have shown this approach to produce insignificant errors). Linearity tests of the camera using an integrating-sphere uniform-luminance standard showed that the linearity rolls off slightly in the top half of the dynamic range, producing a 4% radiance error at the top. To remove this effect, a correction equation is used to correct the CCD to a linear response.

Pixel leakage down rows—row–column cross talk—is also seen in images of high contrast. This leakage could cause Stokes parameter errors for the dim areas of the image. Charge leakage from pixel to pixel during the readout process of the CCD is the probable cause. This row bleeding was found to depend on the width of the bright area, the value of the bright pixels, and the value of the dim pixels. A correction algorithm that iteratively subtracts the bleeding by a constant times the difference of the bright and dim pixels was used to remove this noise with moderate success. Figure 2 shows an example of a high-contrast image before and after the correction.

A. Polarimeter System Matrix Calibration

For each pixel, wavelength, and $f/\#$, calibration was needed to find the actual values of the system matrix, A [see Eq. (2)]. The first three elements of each row of the system matrix can be found by use of a linear polarizer. Images were taken with a large-aperture linear polarizer (extinction ratio better than 10^{-3}) oriented at $-90°$, $0°$, $45°$, and $-45°$ for each polarimeter state with the instrument looking into a 10 cm aperture uniform-luminance standard. This corresponds to the normalized Stokes vectors, [1 1 0 0], [1 −1 0 0], [1 0 1 0], and [1 0 −1 0]. The image values measured at each of these settings were used to determine the first three components of the row. For example, in row 0, a_{00}, a_{01}, and a_{02} were determined, according to Eq. (6).

$$
\begin{aligned}
\text{Image}_{-90} &= 1a_{00} + 1a_{01} + 0a_{02} + 0a_{03},\\
\text{Image}_{0} &= 1a_{00} - 1a_{01} + 0a_{02} + 0a_{03},\\
\text{Image}_{+45} &= 1a_{00} + 0a_{01} + 1a_{02} + 0a_{03},\\
\text{Image}_{-45} &= 1a_{00} + 0a_{01} - 1a_{02} + 0a_{03}.
\end{aligned} \tag{6}
$$

Inspection of Eq. (6) shows that a_{00}, a_{01}, and a_{02} can be determined from these images. Each of the other three rows (a_{1x}, a_{2x}, and a_{3x}) was measured in a similar fashion. The last column of the system matrix could not be measured using only a linear polarizer. Circular polarization states must be used to determine a_{x3}, but because 5 cm diameter zero-order wave plates (for each wavelength) were not available to produce a circular polarization state across the full aperture, the last column of the system matrix was modeled according to the retardances and equivalent rotation angle of each LCVR, assuming they were pure retarders. This measurement of the elements in the first three columns of the system matrix and the modeling of the last column was done for every pixel and every spectral filter at four different $f/\#$'s (2.8, 4.0, 5.6, and 8).

B. Validation of the System Matrix Calibration

Four different polarizer positions of 22.5°, −67.5°, −22.5°, and 67.5° were used to validate the calibration. These states were chosen because they were different from the calibration settings. Unpolarized light was also measured. Finally, circular polarization was created using a 2.5 cm achromatic wave plate. There is uncertainty in the exact Stokes vector obtained with the achromatic wave plate, as the retardance is dependent upon the incidence angle of light and the wavelength, and the exact position of the fast axis changes with wavelength. Nevertheless, an estimate for the accuracy of the fourth column model could be found by measuring light, from the achromatic wave plate. Table 2 shows the maximum errors recorded through all four $f/\#$'s.

The model of the last column of the system matrix seems to cause underestimation of the magnitude of the circular Stokes parameter at 90%. Even with the uncertainties in the achromatic wave plate, higher values of the circular component were expected. For all foreseeable measurements, the light will be partially polarized linear light. If circular light in nature is found, the instrument will measure a circular signature, but not necessarily be quantitatively accurate until we complete the circular polarization calibration with a large-aperture achromatic wave plate. This is acceptable since circular polarization is not expected to be found in either sky or targets. Overall, the linear polarization and unpolarized accuracies seem to be limited by slight exposure jitter in the camera.

Table 2. Summary of Maximum Errors Without Front Lenses

Error	Linear Input (100%)	Unpolarized Input	Circular Input
S_1 and S_2	±1.1%	±0.4%	unknown
S_3	±1.5%	±0.3%	−10%

C. Calibration of Telephoto and Fisheye Lenses

The front lenses, which also alter the Stokes parameters of incident light, were calibrated separately from the polarimeter. Since lenses exhibit very little depolarization[13] and their Mueller matrices are well conditioned, the Mueller matrix of the front lens can be inverted and multiplied by the measured Stokes vector to obtain the input Stokes vector. Calibration of the lenses followed a method that is similar to the system matrix calibration. Using the calibration of the near field with the front lens added, a Stokes vector is measured with a linear polarizer set to −90°, 0°, −45°, and 45°. Using the measured Stokes vectors and the known input Stokes vectors, the first three columns of the lens Mueller matrix were found. Equation (7) shows an example of this calculation for the second row of the Mueller matrix.

$$
\begin{aligned}
S_{1(0)} &= 1m_{10} + 1m_{11} + 0m_{12} + 0m_{13},\\
S_{1(-90)} &= 1m_{10} - 1m_{11} + 0m_{12} + 0m_{13},\\
S_{1(+45)} &= 1m_{10} + 0m_{11} + 1m_{12} + 0m_{13},\\
S_{1(-45)} &= 1m_{10} + 0m_{11} - 1m_{12} + 0m_{13}.
\end{aligned} \tag{7}
$$

Once the first three columns were found, the matrix was assumed to be a symmetric, nondepolarizing Mueller matrix, and the last column calculated. Since the lens is not perfect, use of the nondepolarizing assumption induces some error into the circular component. Most optics have little depolarization,[13] so the measurement of a near-unity matrix is not surprising. A typical Mueller matrix (normalized to m_{00}) is shown in Eq. (8) Notice that calibration errors in the system matrix cause some matrix elements to be slightly greater than unity and the lens matrix measurement compensates for these errors.

$$
\begin{bmatrix}
1.0000 & -0.0006 & -0.0018 & -0.0081\\
-0.0008 & 1.0083 & -0.0047 & 0.0320\\
0.0009 & -0.0019 & 1.0012 & 0.0089\\
-0.0081 & -0.0320 & -0.0089 & 1.0047
\end{bmatrix}. \tag{8}
$$

It should be noted that both lens calibrations were only necessary to measure S_3. If only linear states would be measured, the lens matrices would have been included with the system matrix measurement and the whole system would have been calibrated as a single unit. Use of the model for the fourth column of the system matrix and the use of the symmetrical model for the lens allows a reasonable estimate of S_3.

The fisheye lens is also close to an identity matrix at the center, but slightly worse at high incidence angles. Calibration of the fisheye was accomplished with piecewise measurements across the field of view of the instrument. The luminance standard and polarizer were rotated in a plane defined by the optical axis and the polarizer orientation in the image (as shown in Fig. 3 looking down). The setup shown in Fig. 3 only calibrated a slice across the center of the

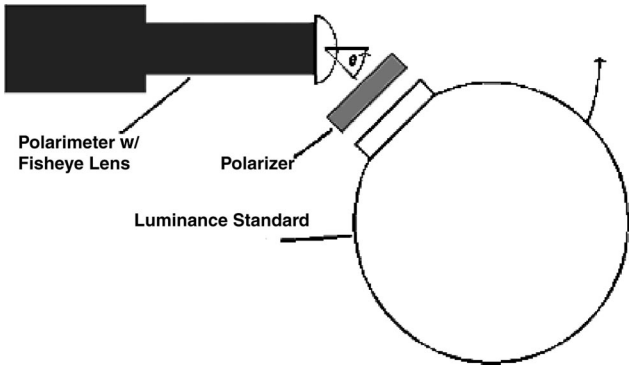

Fig. 3. Setup used in the fisheye lens calibration. The luminance standard and the polarizer rotate together in the direction of the arrow for each calibration piece.

fisheye image. To calibrate the whole image, the polarimeter was rotated −45°, 45°, 0°, and 90° to obtain slices that covered the whole image area.

One problem with the fisheye calibration is the issue of reference plane. The fisheye itself rotates the polarization vector. As an example, consider a fisheye lens viewing the sky dome with the horizon at 90° from the optical axis (because the imager is looking up). The orientation of the polarizer sets the zero-azimuth angle. Horizontal polarization is parallel to the horizon. Light incident from the horizon at 0° azimuth with a *vertical* polarization vector will be measured to have an angle of polarization of 0° by the polarimeter; however, light incident from the horizon at 90° azimuth with *horizontal* polarization also will be measured to have an angle of polarization of 0°. Finally, a field incident upon the fisheye from the horizon at 45° azimuth with a 45° polarization vector will also be measured to have a polarization angle of 0°. Should an incident ray from the horizon that has polarization parallel to the horizon always be measured as the same polarization angle? This is a matter of choice. If all horizontally polarized light at the horizon is measured to have the same polarization angle, there will be a discontinuity at the center, as indicated in Fig. 4. If the rotation of the fisheye is maintained, there will not be a discontinuity, but interpreting angle-of-polarization data is more challenging. Even with this challenge, the latter method was chosen to avoid an additional rotation in the fisheye lens calibration matrix. Postprocessing algorithms could be used to convert between the two types of referencing (i.e., change between horizon reference and instrument-polarizer reference).

Because the fisheye rotated the polarization vector, the calibration polarizer images have a polarization angle that varies across the aperture. Therefore for each piecewise slice, the only accurate angle of polarization was at a line across the center of the slice. For each of the slices, a line was extracted across the accurate part of the calibration slice. Calibration data were then linearly interpolated between each of these calibration lines. In the center of the image (where the polarization aberration was the worst), all the slices converged upon the same calibration so the center was calibrated in a block without interpolation. The accuracy of the interpolation was of concern, but validation discussed below shows that the calibration worked well.

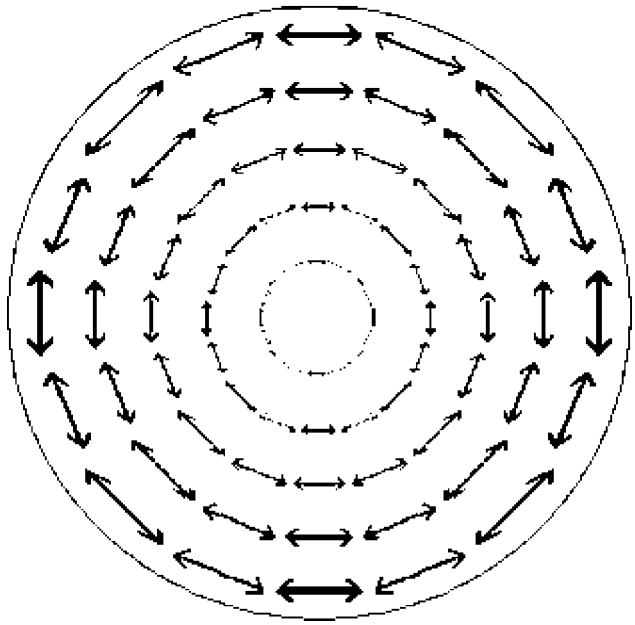

Fig. 4. A discontinuity occurs at the center of the image if all rays with polarization parallel to the horizon are measured as the same polarization angle as shown.

D. Validation of the Lens Calibrations

After calibration of the telephoto lens validation was performed identically to the system matrix validation using 22.5°, −22.5°, 67.5°, and −67.5° polarizer angles. None of the errors in circularly polarized, linearly polarized, or unpolarized light changed significantly. Expected Stokes-vector reconstruction error in the telephoto lens is less than ±1.5% except for S_3.

Fisheye validation used the same method, but multiple validation images were taken across the field of view. For images that were in the interpolated areas, it was difficult to know the exact angle of polarization as it changed across the image of the luminance standard. Nevertheless, the angle of polarization did not seem to depart from what was expected across the center of each image. Errors in the degree of polarization were ±1.5%. Circular errors were significantly worse (±5%) because the circular polarizer models were not entirely valid. Angle-of-polarization error in the center of the fisheye image was ±0.3°. The condition number for the whole imager varied from 1.85 to 2.3 across all $f/\#$'s, wavelengths, and pixels. Therefore depolarization in the LCVRs does not seem to significantly reduce the conditioning of the system matrix.

E. Effects of Using the Wrong $f/\#$ Calibration

As mentioned in Subsection 2.C, the calibration was not expected to remain valid if the $f/\#$ of the system

Table 3. Measurements of Degree of Polarization Over all $f/\#$s Using the $f/4.0$ Calibration

$f/\#$	Measured Degree of Polarization (%)
2.8	99.4
4.0	99.9
5.6	100.3
8.0	100.3

was changed. Therefore to verify this idea, we made measurements at $f/2.8$, $f/4.0$, $f/5.6$, and $f/8.0$, using the calibration for the $f/4.0$ setting. Table 3 shows the average degree of polarization for fisheye measurements obtained with the instrument viewing a linear polarizer oriented at $-22.5°$ for 490 nm as an example. There is clearly a rise in the degree of polarization determined with the $f/4$ calibration as the imager is stopped down. This is expected because setting the instrument at a larger aperture creates more depolarization in the LCVRs. For a set calibration, the lower $f/\#$'s should measure a lower polarization. This confirms the conclusion that each $f/\#$ should be calibrated separately, although in this imager it does not seem to be an excessively large problem. The low incidence angles ($<5°$) probably minimize the problems of depolarization in the LCVRs.

4. Example Data

Images of a clear sky were taken during the afternoon of 17 October 2005 in Bozeman, Montana. The entire region of maximum Rayleigh scattering polarization was visible in the fisheye image. The maximum degree of polarization data are compared against Coulson[1] as a function of wavelength in Fig. 5. Notice that the Bozeman data at 12.5° solar elevation angle compares better with the Mauna Loa data at 45° solar elevation angle. Since the elevation of Mauna Loa is approximately 3353 m and that of Bozeman is approximately 1524 m, it expected that a thicker atmosphere, higher aerosol loading, and terrain reflectivity differences could cause the ~4% difference between the data sets. Sky clarity could also be an issue; over the course of the afternoon, some clouds were seen in the vicinity of the mountains around Bozeman. Initial data has shown that even small clouds at any point in the sky are strongly correlated with a reduction of the maximum degree of polarization, even if the cloud is located a long way from the area of maximum degree of polarization. The maximum degree of linear polarization (DOLP) at longer wavelengths seems to be affected more by clouds than short wavelengths (Fig. 6).

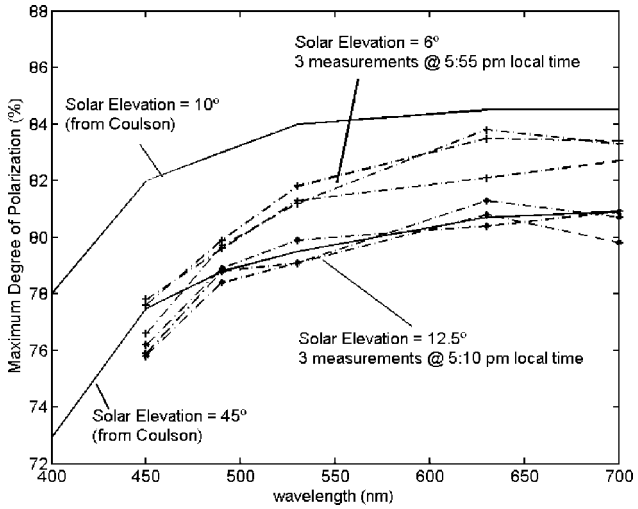

Fig. 5. Maximum degree of polarization observed in clear sky data (Bozeman, Montana, 17 October 2005) compared with Coulson's data (Ref. 1, p. 285).

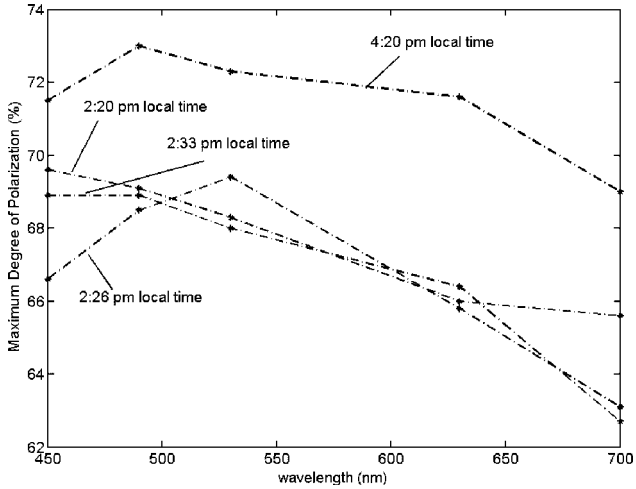

Fig. 6. Reduction of polarization at longer wavelengths when clouds are seen in the sky (Bozeman, Montana, 18 October 2005).

Figure 7 shows examples of full-sky data for a clear sky at 450 nm wavelength. Slight artifacts from the fisheye calibration may be visible in the center of the DOLP image. Since the DOLP is relatively low in the center, the artifacts are barely visible in the original image. Random dark noise causes some striping in the DOLP image. Although visible in the original images, this error is still small compared with the overall systematic error discussed above. The Babinet neutral point is clearly visible at the intersection of the angle of polarization (AOP) lines. The green area to the right of the point is an overexposed area around the Sun. The block-shaped areas and adjacent objects are rooftop structures with radio antennas. The Sun itself is behind these buildings, thereby eliminating concern over lens flare and CCD blooming.

When clouds are visible, the DOLP becomes smaller, but the band of maximum degree of polarization across the sky is still visible (Fig. 8). For liquid clouds, the angle of polarization does not change, in agreement with previous work.[14] Initial data show that clouds near the solar point at sunset may change the angle of polarization, which will be investigated in a future work.

Figure 9 shows DOLP and AOP images of a partly cloudy sky at 700 nm, taken within 20 s of the

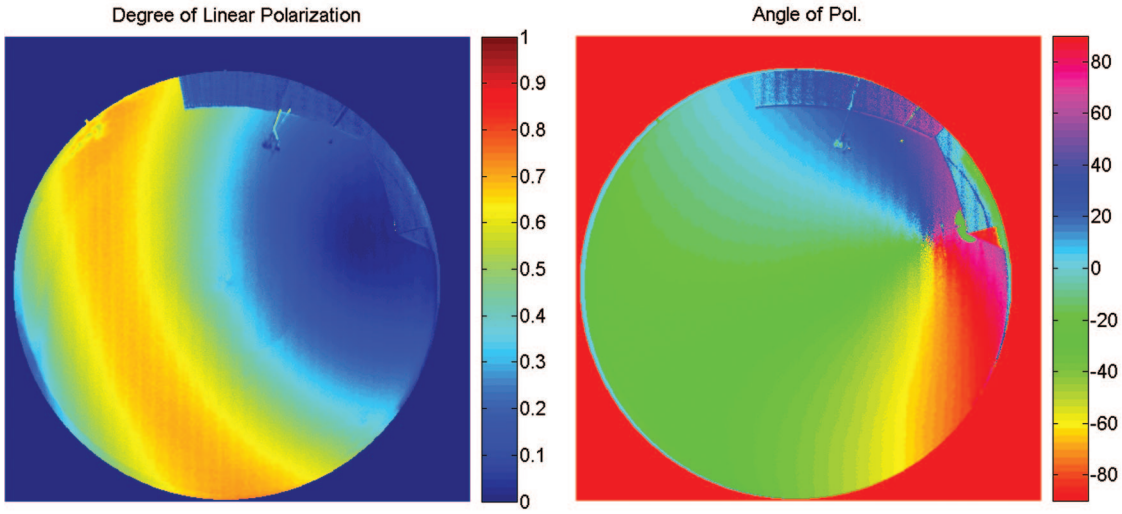

Fig. 7. Clear-sky polarization at 450 nm (18 October 2005, 2:13 p.m. MDT).

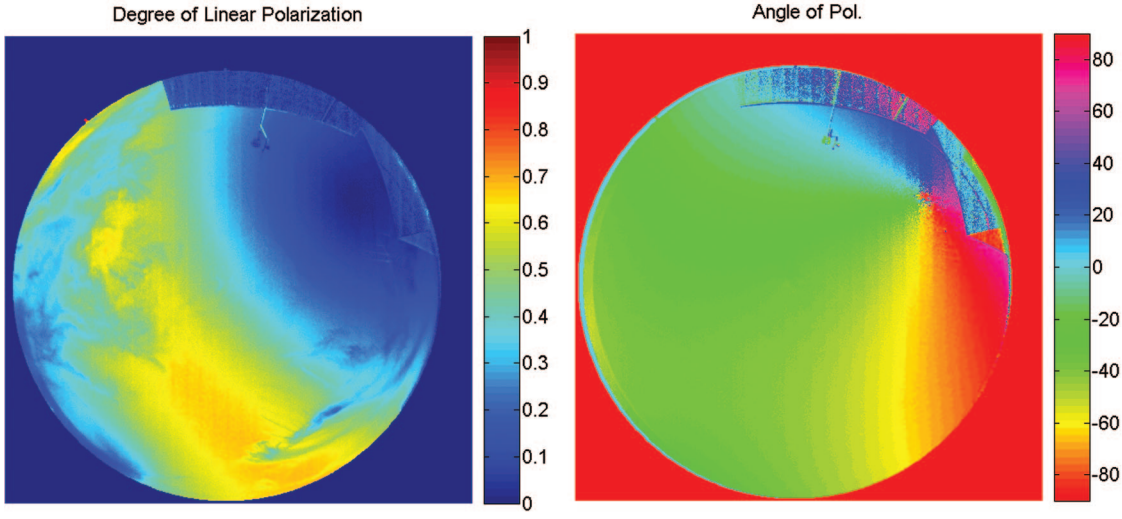

Fig. 8. Partly cloudy sky polarization at 450 nm (18 October 2005, 3:08 p.m. MDT).

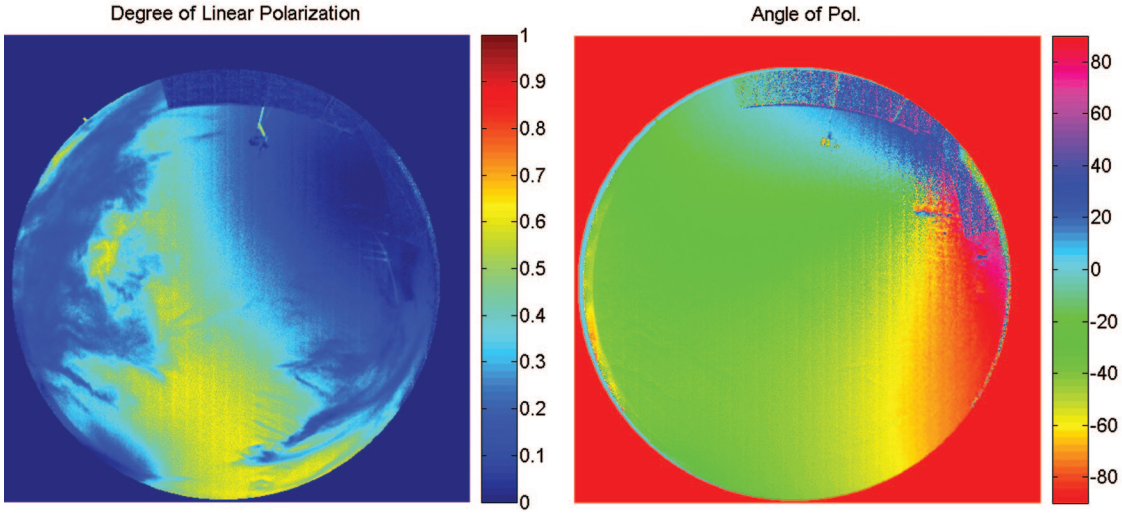

Fig. 9. Partly cloudy sky polarization at 700 nm (18 October 2005, 3:08 p.m. MDT).

450 nm images. The longer-wavelength DOLP is affected more by clouds, resulting in clouds that are seen with better contrast (Fig. 9 compared to Fig. 8). Also, notice that the DOLP of the clear sky between the clouds is reduced significantly for the longer wavelength. For 700 nm, the clear-sky DOLP is normally greater than the 450 nm DOLP, but with clouds it is less. It remains to be seen whether this is caused by higher aerosol concentrations in this area of the sky, or if the distant clouds are changing the clear-sky polarization through multiple scattering (see also Fig. 6 for similar results).

5. Summary and Conclusions

We have described the development, calibration, and validation of a dual-field imaging polarimeter designed for measuring the effect of varying sky polarization on the polarization signatures of ground-based objects. This system employs liquid crystal variable retarders to rapidly vary the polarization state of the measurements to minimize errors caused by changing sky conditions. By calibrating each pixel at every wavelength and $f/\#$, we are able to compensate for the incidence-angle dependence of LCVR retardance. The system is being used to study sky polarization as a function of variable cloudiness. Initial data show good agreement with previous measurements for clear skies and show that clouds can alter the polarization of light in clear parts of a partly cloudy sky. More detailed analysis of these effects is the subject of our ongoing studies.

This material is based on research sponsored by the Air Force Research Laboratory, under agreement FA9550-04-1-0037. The U.S. Government is authorized to reproduce and distribute reprints for governmental purposes notwithstanding any copyright notation thereon. The views and conclusions contained herein are those of the authors and should not be interpreted as necessarily representing the official policies or endorsements, either expressed or implied, of the Air Force Research Laboratory or the U.S. Government.

References

1. K. L. Coulson, *Polarization and Intensity of Light in the Atmosphere* (Deepak Publishing, 1988).
2. G. Horvath, A. Barta, J. Gal, B. Suhai, and O. Haiman, "Ground-based full-sky imaging polarimetry of rapidly changing skies and its use for polarimetric cloud detection," Appl. Opt. **41,** 543–559 (2002).
3. J. North and M. Duggin, "Stokes vector imaging of the polarized sky-dome," Appl. Opt. **36,** 723–730 (1997).
4. K. Voss and Y. Liu, "Polarized radiance distribution measurements of skylight. I. System description and characterization," Appl. Opt. **36,** 6083–6094 (1997).
5. Y. Liu and K. Voss, "Polarized radiance distribution measurement of skylight. II. Experiment and data," Appl. Opt. **36,** 8753–8764 (1997).
6. K. Suzuki, "Lens capable of short distance photographing with vibration reduction function," U.S. Patent 5,751,485 (12 May 1998).
7. S. Sato, "Internal focusing type telephoto lens," U.S. Patent 5,757,555 (26 May 1998).
8. H. Sato, "Fisheye-lens having a short distance compensating function," U.S. Patent 5,434,713 (18 July 1995).
9. D. S. Sabatke, M. R. Descour, and E. L. Dereniak, "Optimization of retardance for a complete Stokes polarimeter," Opt. Lett. **25,** 802–804 (2000).
10. J. S. Tyo, "Noise equalization in Stokes parameter images obtained by use of variable retardance polarimeters," Opt. Lett. **25,** 1198–2000 (2000).
11. J. S. Tyo, "Design of optimal polarimeters: maximum of signal-to-noise ratio and minimization of systematic error," Appl. Opt. **41,** 619–630 (2002).
12. X. Xiao, D. Voelz, and H. Sugiura, "Field of view characteristics of a liquid crystal variable retarder," in *Polarization Science and Remote Sensing,* J. A. Shaw and J. S. Tyo, eds., Proc. SPIE **5158,** 142–150 (2003).
13. R. Chipman, "Depolarization index and the average degree of polarization," Appl. Opt. **44,** 2490–2495 (2005).
14. I. Pomozi, G. Horvath, and R. Wehner, "How the clear-sky angle of polarization pattern continues underneath clouds: full-sky measurements and implications for animal orientation," J. Exp. Biol. **204,** 2933–2942 (2001).